P13.3 KINEMATIC AND THERMODYNAMIC VARIABILITY IN THE SUPERCELL ENVIRONMENT OBSERVED USING STICKNET

Joel Dreessen*
Texas Tech University, Lubbock, Texas

Christopher C. Weiss
Texas Tech University, Lubbock, Texas

1. INTRODUCTION AND MOTIVATION

Kinematic boundaries, as defined by sharp wind shifts, have been implicated in type-II tornadogenesis in numerous studies (e.g., Wilson 1986; Brady et al. 1989; Roberts and Wilson 1995). Pockets of vertical vorticity are typically observed along these boundaries, which can then be stretched by updrafts to amplify rotational velocity. Vortices of this nature have been observed (e.g., Pietrycha and Rasmussen 2004; Murphey et al. 2006) and simulated (e.g. Lee and Wilhemson 1997a). These pockets of vorticity, called misocyclones (Fujita 1981), have a spectrum of sizes, ranging from landspouts to dust devils, and form in differing environmental conditions. Relatively quiescent boundaries, such as those found in the Denver Convergence and Vorticity Zone or stationary drylines, produce vortices (Pietrycha and Rasmussen 2004). Numerical simulations and observations of misocyclones also suggest that they can be generated on advancing outflow boundaries. The rear flank downdraft (RFD) of supercells produces an outflow boundary known as the rear flank gust front (RFGF). Conditions along this boundary are often conducive for misocyclone formation.

During the spring of 2008, Texas Tech University, in collaboration with the University of Michigan, conducted the Multiple Observations of Boundaries In the Local Storm Environment field project (MOBILE_2008). Using StickNet (SN), the rapidly deployable observation network newly-developed by Texas Tech, detailed observations of the surface thermal and kinematic variability of thunderstorm outflows were attained with attention focused on the RFD. The purpose of this study is to document the conditions and variability along the RFGF and investigate the presence of pre-tornadic circulations 1-4 km in size along the RFGF and their possible contribution to tornadogenesis.

* *Corresponding author address: Joel A. Dreessen, Texas Tech University, Atmospheric Science Group, Department of Geosciences, Lubbock, TX, 79409; e-mail: Joel.Dreessen@ttu.edu*

2. METHODOLOGY

To adequately assess the relevance of the data collected for this study, SN placements were overlaid on WSR-88D reflectivity (Figure 1). Those platforms in close proximity of radar-identified mesocyclones or visually reported phenomenon (e.g., funnel cloud) were examined in greater detail. Using the time series collected at these platforms, wind discontinuities identifying the RFGF are noted while paying special attention to higher-order variability within the RFGF zone. Concurrent analysis of pressure and temperature variability is used to deduce whether a misocyclone transversed the platforms. A particularly useful method for identifying rotation is observing opposite directional trends in winds at adjacent platforms. For example, if a cyclonically rotating misocyclone were to pass between two platforms, backing and veering winds would occur at the north and south platforms, respectively.

Radar data, when available, are incorporated into the analysis to assist in the determination of possible misocyclones. The presence of misocyclone-scale vertical vorticity can be inferred from couplets in instantaneous radial wind velocity and time-to-space converted SN observations. The translation and evolution of these vertical vorticity maxima are estimated by creating time series of these observations so their position and motion relative to developing tornadoes can be measured.

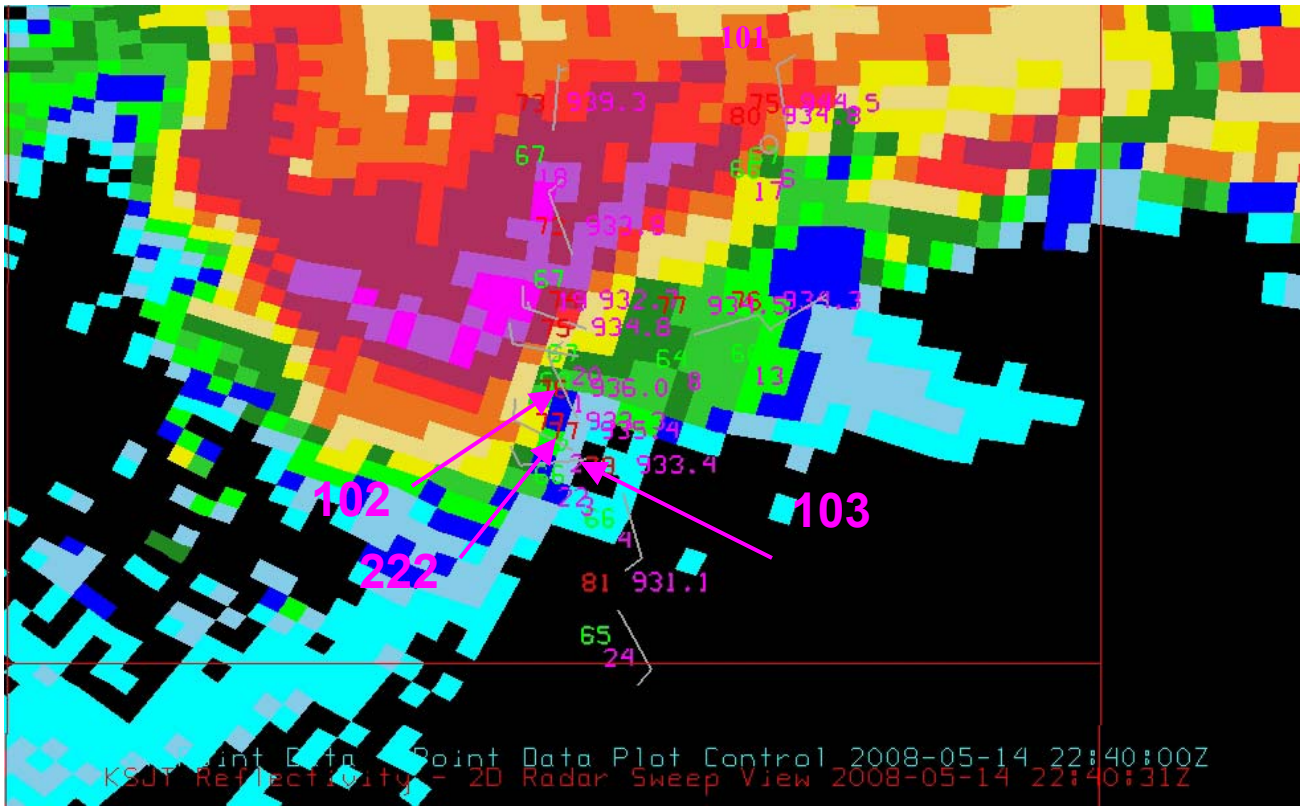

FIG. 1 – WSR-88D 0.5 degree reflectivity with StickNet locations overlaid. StickNet data are shown in a METAR format. Wind is in knots, temperature and dewpoint are in Fahrenheit. Bottom number gives truncated platform identification. Platforms discussed in the text are marked with an arrow.

3. CASE STUDY

The deployment of SN near Eden, TX on May 14, 2008 produced an interesting data set of a rapidly evolving HP supercell. Overlays of SN data and radar imagery show the relevant platforms and their proximity to storm features as previously described (Figure 1). In time series, a general backing of winds in probe 102 and general veering in probes 222 and 103 were clearly evident (Figure 2). While stations farther to the north and south outside the selected window have backing and veering winds, respectively, they do not shift as dramatically as seen in the time series of platforms 102, 222, and 103. The wind shift takes approximately three minutes to complete; assuming a storm motion of 65km/hr(~40mph), as calculated from WSR-88D animations, such a circulation translating through the SN array would be just less than 3 km in diameter.

The Doppler on Wheels (DOW) radar was scanning in close proximity to the storm and the SN array. Reflectivity imagery shows a very pronounced "hook-like" feature on the front (east) side of the storm (Figure 3). Radial velocity (Figure 4) confirms the presence of convergent cyclonic shear along a sharp kinematic gradient. The scale of the feature in figures 3 and 4 is approximately 2 km in diameter (range rings have 2 km spacing), approximately the same order scale as calculated using the SN time series and estimated storm velocity.

Time-to-space calculations also confirm a sense of cyclonic rotation of approximately the same size as the calculations above (Figure 3). Time-to-space conversion covers a three minute time period from 22:37Z to 22:40Z showing averaged wind values every ten seconds. The time-to-space analysis does not coincide with the radar “hook” as seen in figure 3, suggesting a possible second area of cyclonic vorticity.

A thermodynamic deficit lags the initial wind shift of the RFGF by about five minutes (Figure 2). However, the RFD eventually shows extreme thermodynamic deficits (~10K). This five minute lag in thermodynamic response puts the apparent circulation approximately 2-3 minutes ahead of the cold pool. Assuming again a storm motion of approximately 40 mph, this location is just over 1km east of the cold pool.

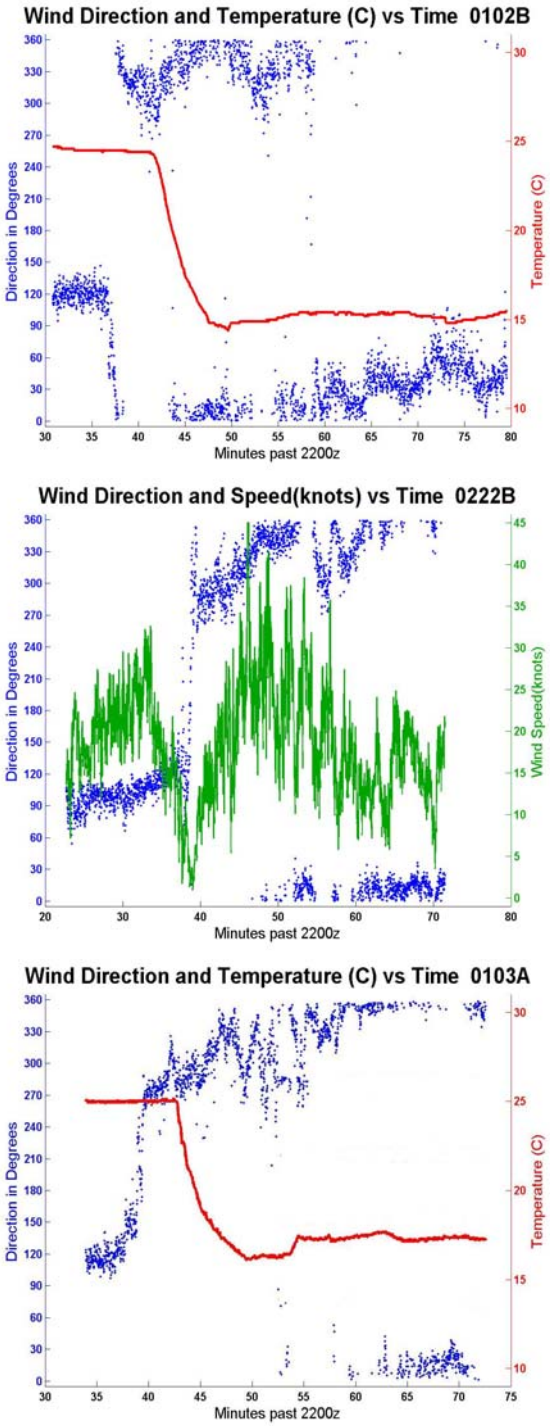

FIG. 2 – A collection of time series from platforms 102, 222, and 103, from north to south is displayed with minutes past 22Z on the x-axis. Blue dots represent the instantaneous measurements of wind direction. Notice the contrasting backing winds of 102 with the veering winds of 222 and 103. 102 and 103 also display temperature in Celsius as a function of time. Platform 222 displays wind velocity, in knots, and is representative of the other two platforms.

It should be noted that the storm produced a tornado approximately 20 minutes after passing through the selected window where one SN probe far to the east captured the RFD near the developing tornado.

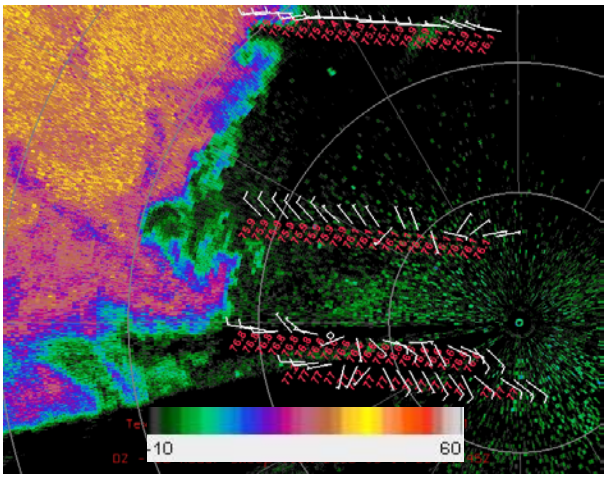

FIG. 3 – PPI Display of reflectivity as observed by the DOW radar. Range rings have 2 km spacing. The radar is centered just below center on the right. Time of the image is 22:37:45Z. Time-to-space conversion for the three platforms discussed above is plotted every 10 seconds from 22:37:00Z to 22:40:00Z. Numbers in red are temperature in Fahrenheit. DOW is stationary during this image. Wind barbs are in knots.

4. SUMMARY AND FUTURE GOALS

During spring of 2008, MOBILE_2008 conducted research using StickNet platforms developed by Texas Tech. This instrumentation intercepted multiple supercell thunderstorms during the course of the project. Presented here is the preliminary analysis of one such deployment near Eden, TX on May 14, 2008.

Additional cases exist and await analysis. While much of the current work is preliminary, analyzing more cases with the methodology defined above will expand the current understanding of misovortex dynamics. Moreso, should a sufficient number of misovortex observations be found, some conclusions could be drawn concerning the thermodynamic and kinematic conditions generating misocyclones in the supercell environment. Inferences pertaining to the influence of misocyclones in supercell tornadogenesis will also be attempted.

A complete study of this phenomenon can more easily be accomplished in the future with the addition of the newly-developed Texas Tech Ka-

band (TTUKa) radars. Since misocyclones often occur in the absence of hydrometeors, the high sensitivity of the TTUKa platforms will aid in their detection.

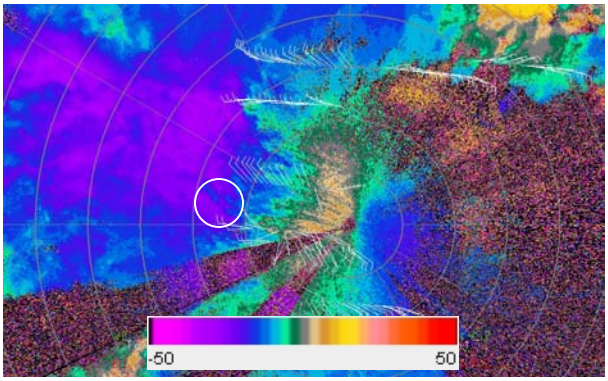

FIG. 4 – As in figure 3 except for radial velocity (m/s). Wind barbs are in knots. The white circle identifies the area of the "hook" seen in figure 3. Some cyclonic shear exists in this area. A second area of shear seems to be nearly collocated with the turning of the winds seen in the time-to-space plots.

6. ACKNOWLEDGEMENTS

The authors are grateful to Josh Wurman and the DOW group for the radar images and to all participants in the spring MOBILE_2008 project for their hard work and dedication.

7. REFERENCES

Brady, Raymond H., and Szoke, Edward J., 1989: A case study of nonmesocyclone tornado development in northeast Colorado: Similarities to waterspout formation. *Mon. Wea. Rev*., **117**, 843-856.

Fujita, T. Theodore, 1981: Tornadoes and downbursts in the context of generalized planetary scales. *J. Atmos. Sci*., **38**, 1511-1534.

Lee, B. D. and R. B. Wilhelmson, 1997: The numerical simulation of non-supercell tornadogenesis. Part I: Initiation and evolution of pretornadic misocyclone circulations along a dry outflow boundary. *J. Atmos. Sci*., **54**, 32-59.

Murphey, H. V., R. M. Wakimoto, C. Flamant, D. E. Kingsmill, 2006: Dryline on 19 June 2002 during IHOP. Part I: Airborne Doppler and LEANDRE II analyses of the thin line structure and convection initiation. *Mon. Wea. Rev*., **134**, 406-430.

Pietrycha A. E. and E. N. Rasmussen, 2004: Finescale surface observations of the dryline: A mobile mesonet perspective. *Wea. Forecasting*, **19**, 1075-1088.

Roberts, R. D., J. W. Wilson, 1995: The genesis of three nonsupercell tornadoes observed with dual-doppler radar. *Mon. Wea. Rev*., **123**, 3408-3436.

Wilson, J. W., 1986: Tornadogenesis by nonprecipitation induced wind shear lines. *Mon. Wea. Rev*., **114**, 270-284.